Electrode-dependent asymmetric conduction mechanisms in $K_{0.5}Na_{0.5}NbO_3$ micro-capacitors

C. Groppi [a], F. Maspero [b,c], A. Rovelli [a], M. Asa [d], G. Malavena [e], C. Monzio Compagnoni [e], E. Albisetti [a], S. Vangelista [f], M.A. Badillo-Ávila [a,*], R. Bertacco [a]

[a] *Department of Physics, Politecnico di Milano, Piazza Leonardo da Vinci 32, 20133, Milano, Italy*
[b] *Department of Environmental and Civil Engineering, Politecnico di Milano, Piazza Leonardo da Vinci 32, 20133, Milano, Italy*
[c] *CNR Istituto di Fotonica e Nanotecnologie, Politecnico di Milano, Piazza Leonardo da Vinci 32, 20133, Milano, Italy*
[d] *Polifab, Politecnico di Milano, Via G. Colombo 81, 20133, Milano, Italy*
[e] *Department of Electronics, Information and Bioengineering, Politecnico di Milano, Piazza Leonardo da Vinci 32, 20133, Milano, Italy*
[f] *STMicroelectronics, Via Camillo Olivetti 2, 20864, Agrate Brianza MB, Italy*

ARTICLE INFO

ABSTRACT

The ultimate performance of devices employing lead-free piezoelectrics is determined not only by the intrinsic properties of the piezo, but also by processes and materials employed to create the electric contacts. In this paper, we investigate the impact of different metallic electrodes with increasing chemical reactivity (Pt, Ni, Ti, Cr), on the asymmetric behavior of the leakage current in $M/K_{0.5}Na_{0.5}NbO_3/Pt(111)$ micro-capacitors, where M stands for the top metallic electrode. For all electrodes we found a marked leakage asymmetry that we ascribed to the presence of a Schottky-like rectifying junction at the $M/K_{0.5}Na_{0.5}NbO_3/Pt(111)$ bottom interface, while the corresponding junction at the top interface is deeply affected by the creation of oxygen vacancies due to oxygen scavenging during the growth of the top metallic electrodes, leading to an almost ohmic top contact. The leakage increases with the reactivity of the electrodes, while the asymmetry decreases, thus suggesting that the creation of the top metal/$K_{0.5}Na_{0.5}NbO_3$ interface generates oxygen vacancies diffusing down to the bottom interface and impacting on the rectifying behavior of the Schottky-like junction. Noteworthy, this asymmetric conduction can reflect in an asymmetric piezoelectric and ferroelectric behavior, as a sizable portion of the applied voltage drops across the rectifying junction in reverse bias, thus hampering symmetric bipolar operation, especially in leaky materials.

1. Introduction

In the field of lead-free piezoelectric ceramics, thanks to its high d_{33} values (570 pC/N) [1], potassium sodium niobate (KNN) has emerged as a suitable candidate to replace lead zirconate titanate (PZT) as a ferroelectric and piezoelectric material. Despite the remarkable advancements in fabrication of KNN bulk ceramics in the last few decades, applications of KNN in thin film form are still at the early stage and currently represent a hot topic of research. Several aspects of KNN films fabrication still need to be optimized, such as the precise control of stoichiometry, doping with suitable elements, formation of ternary compounds with other metal oxides, proper deposition parameters for fabrication of uniform and highly textured films, etc. In addition, a full understanding of the conduction and loss mechanisms in thin films, as

well as of the electrical response at varying frequencies is still lacking [2, 3]. This said, the understanding and solution of problems related to KNN films is extremely compelling as it could make possible their application in the area of green and biocompatible micro- and nano-electromechanical systems (MEMS and NEMS). KNN, and some other lead-free ferroelectrics and piezoelectrics, hold promise for small sensors, actuators, lab-on-a-chip electronics, and memory devices with high energy efficiencies. If thin film deposition and device fabrication processes are made cost-effective and affordable for the industrial sector, KNN could be deployed on a large scale and partially replace lead zirconate titanate (PZT) which is one of the most widely used piezoelectric ceramic materials in the world. Interestingly, apart from better resistance to fatigue with respect to PZT, KNN is also non-toxic, which makes it biocompatible and thus opens an exciting door for research in

---

biosensors and bio-energy harvesters [4–7]. Regarding full device fabrication, however, also other ancillary materials needed for efficient operation of KNN-based electronics are as important as the piezoelectric itself. In particular, the choice of suitable electrode materials is crucial as the bottom electrode deeply influences the film texture and morphology, while both top and bottom electrodes determine the leakage and linearity of the piezo-response.

Typically, due to its extremely good chemical resistance to oxidation and its high work function, platinum is chosen as a metal electrode. Besides, Pt(111) produces the desired preferential (001) orientation of KNN grains. Nevertheless, Pt is a rather expensive metal, which can largely influence the final cost of KNN based devices. Therefore, the use of Pt should be avoided, or at least limited. Although there are cheaper alternatives to platinum, the reliability of other metal electrodes might compromise the operation of KNN devices. Thus, proper evaluation of such other metal electrodes is necessary. In a previous report of ours, we have demonstrated piezoelectric properties of KNN when deposited by pulsed laser deposition (PLD) on Pt bottom electrodes and topped with Ti [8].

In a recent and interesting report, Shweta et al. [9], explored the effect of several top electrodes for KNN with a common Pt bottom electrode. They have used Pt, Pd, Au, Cr and Al. The metal work function of such elements decreases in the order described. Nonetheless, the leakage does not follow exactly the same trend. They observed rectifying behavior for Al, Cr and Au top electrodes, and ascribed it only to a difference between work function of top and bottom electrode material. For Pt and Pd top electrodes they found a symmetric behavior of J vs E, which was explained by d-shell occupancy of the metals. The possible role of oxygen vacancies was not taken into account in their work. A similar leakage asymmetry has been observed for other metal-oxide-metal devices [10–12] and it was also found in piezoelectric stacks both for PZT [13–15] and KNN films [9,16,17].

For the present work, Pt, Ni, Ti and Cr were employed as top electrodes of a KNN–Pt stack to fabricate metal-insulator-metal capacitors (MIM). For comparison, a common Pt(111) bottom electrode to all stacks was used as template for deposition of KNN by Pulsed Laser Deposition (PLD) [8]. Highly asymmetric J-E behavior was observed for all the fabricated devices. However, at variance with the study of Shweta et al., we found that the Pt–KNN–Pt and Ni–KNN–Pt stacks produced the most pronounced rectification. For Ti and Cr electrodes the asymmetry was much less important, but the high leakage points to a high oxygen vacancies concentration in the bulk of KNN and close to the interfaces. The fact that the more pronounced rectifying behavior was found for a symmetric Pt/KNN/Pt stack indicates that the leakage asymmetry is not due to asymmetric barriers at top and bottom interfaces simply connected to the different work function of the electrodes. In our samples, a careful analysis of the leakage and small-signal capacitance indicates that the bottom and top interface behave as a rectifying Schottky junction and as an almost ohmic contact, respectively. We interpret this behavior as the result of the creation of oxygen vacancies, acting as dopants, due the scavenging of oxygen by metals deposited on KNN to create the top electrode, whose reactivity is enhanced due to the formation of metallic nanoparticles at the early stage of metal growth on oxides. Even though this mechanism can be peculiar to the specific processes used for KNN and electrode deposition, thus justifying some discrepancies with previous works, our results point out to the relevance of oxygen scavenging by metallic electrode materials in determining the final performances of piezo-devices.

2. Materials and methods

2.1. Pulsed laser deposition of KNN on platinized silicon substrates

For removal of possible organic residuals from platinized silicon substrates (Pt(100 nm)/TiO$_2$(20 nm)/SiO$_2$(700 nm)/Si), an ex-situ oxygen plasma cleaning for 10 min was performed before the PLD process.

To promote platinum template surface stabilization and coalescence, in-situ vacuum annealing was performed at 615 °C for 90 min with a final pressure of 5×10^{-5} Pa. The fine tuning of the PLD deposition of KNN has been reported in past works of ours [8]. The target substrate distance was fixed at 35 mm, and the deposition temperature of the substrate was held at 615 °C with a constant oxygen pressure of 29.3 Pa. 300 nm of KNN were deposited at a rate of 2.73 nm/min, leading to a deposition time of 110 min. Right after deposition, the samples were annealed in-situ at 500 °C for 30 min to promote crystallization. Top electrodes were deposited as matrices of squared pads (38 × 38 μm^2) on top of KNN. Nickel, titanium and chromium were deposited by metal evaporation, while platinum was deposited by magnetron sputtering. All the matrices of pads were deposited using a physical shadow mask.

2.2. Device characterization

Electrical measurements were carried out in top-bottom configuration, with one tip of the probe station in contact with the top electrode (biased) and the other tip in contact to the bottom Pt layer (grounded). Current-voltage (leakage) curves were obtained with a Keithley 2612 System voltage source on a SUSS MicroTec PM5 probe station. Time of Flight Secondary Ion Mass Spectrometry (ToF-SIMS) of the different M-KNN-Pt/TiO$_2$ stacks was performed in an IONTOF M6 plus equipment, located at STMicroelectronics Physical Laboratory. Depth profiling was performed in the dual beam mode. Measurements were done with a 15 keV Bi$^+$ beam for analysis, and 1 keV Cs$^+$ as sputter beam. This condition allows to enhance the negative ions signals as oxide complexes (i.e. M − O complexes). The sputter beam size was of 300 × 300 μm^2; the analysis area was 50 × 50 μm^2.

Capacitance measurements were done with a LCR meter (Keysight E4980A). Topography and conductive atomic force microscopy (C-AFM) measurements were performed with a Park NX10 AFM by Park Systems. For this set-up, the common bottom Pt electrode was biased, while a scanning diamond tip was grounded.

3. Results

The KNN capacitors, made of a common bottom Pt electrode and different top metal electrodes (Pt, Ni, Ti, Cr), were tested electrically to determine their J-E characteristics, where J is the current density and E the electric field estimated as the voltage applied to the top electrode with the bottom electrode grounded (V$_{TB}$) divided by the KNN film thickness. As shown in Fig. 1, all devices present highly asymmetric
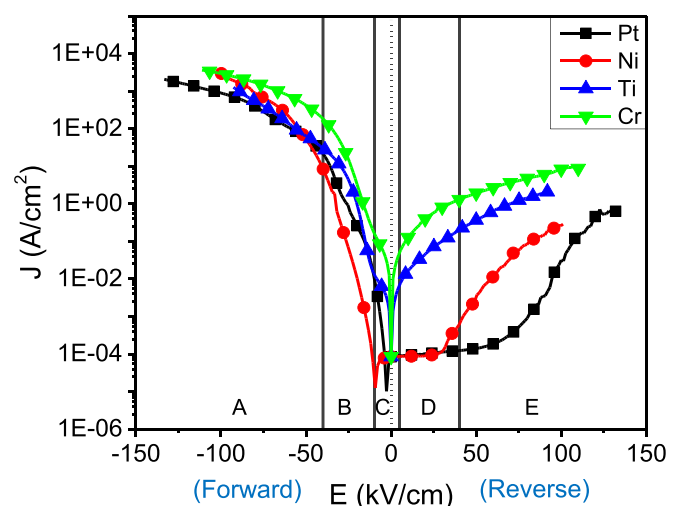

Fig. 1. Current density versus electric field for different top electrode materials for KNN/Pt stacks.

curves. In particular, a high current was measured for all stacks when the top electrode was negatively biased. For the positive bias, the current was smaller by orders of magnitude, with a clear dependence on the material of the top electrode. Due to the observed rectifying behavior, in the following we will identify these two regimes as "forward-bias" ($V_{TB} < 0$) and "reverse bias" ($V_{TB} > 0$). Looking in more detail at the J-E curves, we can distinguish five regimes indicated by capital letters in Fig. 1. For small bias, the semi-log plot displays a symmetric dip (region C) with almost linear J-E characteristic for Cr and Ti electrodes, which can be ascribed to a low-bias ohmic regime where charge transport is given by thermally activated carriers in the conduction or valence band of KNN, regarded as a large gap semiconductor ($E_g = 3.5$ eV) [18,19]. For Pt and Ni, we find a similar behavior in about 50% of tested micro-capacitors, while in the rest of cases, like that shown in Fig. 1, a clear asymmetry appears also at low bias, with lower leakage current for $V_{TB} > 0$. The fact that the minimum leakage in some devices is not found at zero bias indicates the presence of trapped charges [20,21]. Moving to larger positive bias, the difference between Pt–Ni and Cr–Ti becomes more evident. Pt and Ni curves display a plateau (region D) up to an electric field on the order of 30–50 kV/cm, after which the current sizably increases (region E), still remaining at least three orders of magnitude lower than that for the corresponding negative bias. For Ti and Cr we just see a moderate increase of J, without any plateau. For the opposite polarity ($V_{TB} < 0$) we assist to a steep increase of J (region B) up to about −40 kV/cm, when the slope decreases (region A).

Commonly, asymmetric currents in MIM devices are explained on the basis of the different metal work functions and filled state of d-shell of the employed elements for the electrodes [9,17]. Although this interpretation is well based, there are other aspects to be considered. For instance, the rectifying behavior observed in our devices is established even for the chemically symmetric Pt/KNN/Pt MIM stack. This indicates that, although the nominal work function is the same, the top and bottom interfaces are substantially different from one another, as also shown in previous works on PZT [13–15]. The phenomenon is typically attributed to the presence of oxygen vacancies with different concentration in the vicinity of the metal-insulator contacts [16,22], thus leading to the creation of a net effective potential barrier in MIM devices acting asymmetrically on the transport of charges [11,12,20].

To check the validity of this model, we performed a typical characterization of metal-semiconductor junctions, i.e. the measurement of the small signal capacitance as a function of applied bias. Owing to the more asymmetric behavior and small reverse current in the case of micro-capacitors with Pt and Ni electrodes, such stacks were tested. A small AC signal (50 mV, 10 kHz) was applied on top of a variable $V_{TB} > 0$ DC bias, (in the reverse-bias condition, where the leakage current is small enough to allow for reliable capacitance measurements) while measuring the complex impedance with a LCR meter (Keysight E4980A). In Fig. 2a, we plot the inverse of the square of the small capacitance ($1/C^2$) versus the applied voltage V_{TB}, which indeed displays the linear behavior expected for a Schottky junction. Note that this is very different from an ideal dielectric capacitor where the capacitance should be almost independent on the bias: in our case, the applied small signal mainly drops on the capacitance associated to the space-charge region. As derived from Schottky theory, $1/C^2 = 2(\varphi_{bi}-V_a)/(q \cdot \varepsilon \cdot N_d)$, where φ_{bi} is the built-in voltage, V_a is the voltage applied to the metal with the semiconductor grounded, q the electron charge, ε the dielectric constant, and N_d the density of donors in case of a n-type semiconductor. The reasons why we assume a n-type behavior of KNN are discussed below but are mainly related to oxygen vacancies acting as donors. Noteworthy, $1/C^2$ increases moving towards large $V_{TB} > 0$, which according to the above equation should correspond to $V_a < 0$, i.e. a negative voltage drop between the metallic electrode and KNN. In our structure, this condition applies only to the bottom KNN/Pt(111) interface, thus pointing towards the fact that the rectifying behavior is determined by the bottom interface. Note that the calculated built-in biases from the intercept with the bias voltage in Fig. 2a, namely 1.2
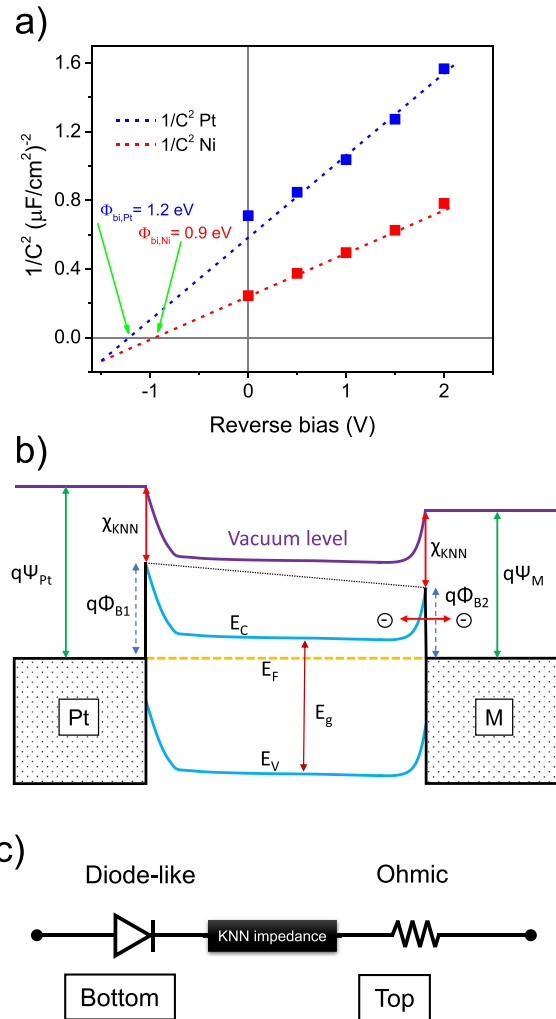

Fig. 2. a) graph of $1/C^2$ vs V as used in the model of a Schottky-semiconductor diode interface. b) qualitative band-structure scheme for the metal-semiconductor-metal stack (platinum-KNN-top metal) at zero bias. c) Simplified electrical model of the Pt–KNN-top metal stack. The capacitive contributions are not represented.

eV for Pt and 0.9 eV for Ni, are in agreement with the general trend expected from the values of the work function of the two metals ($\Psi_{Pt} \sim$ 5.65 eV, $\Psi_{Ni} \sim$ 5.15 eV). Even though the absolute values of the built-in potential cannot be derived from a classical model considering a uniform doping throughout the KNN film and no interface states, these findings support the reliability of our model.

In Fig. 2b), we report a sketch of a qualitative band diagram of KNN micro-capacitors for zero applied bias, which is consistent with our measurements. KNN is a dielectric ceramic and there is very little quantitative data on its behavior as a "wide-gap semiconductor" ($E_g = 3.54$ eV) [18,19]. However, it is well known that KNN is highly prone to n-type or p-type doping by oxygen vacancies and alkaline vacancies, respectively, which typically originate during deposition and processing. The overall balance can make of KNN an n-type or p-type semiconductor [23]. More typically, KNN has been reported as a n-type semiconductor due to oxygen vacancies [24,25]. The qualitative band alignment depicted in Fig. 2b) is obtained assuming a n-type doping, which is coherent with the fact that the overall scenario from our experimental data can be explained in terms of creation of oxygen vacancies due the scavenging action by metals deposited on KNN, as explained below. At the bottom interface, due to the large work function

of Pt ($\Psi_{Pt} \sim 5.65$ eV) compared to the sum of the KNN energy gap ($E_g = 3.54$ eV) and electron affinity (χKNN ~ 1.1 eV similarly to other niobates) [26], we expect that the Fermi level alignment of Pt and KNN involves the transfer of electrons from KNN to Pt. This also leads to an upwards band bending and subsequent space charge accumulation due to oxygen vacancies acting as point defect donors. As mentioned above, the precise entity of the Schottky barrier height (Φ_B) and built-in potential (φ_{bi}) cannot be determined using the simple Schottky model ($\Phi_B = \Psi_{Pt} - \chi$, $\varphi_{bi} = \Phi_B - E_c + E_F$) due to the well-known phenomenon of Fermi level pinning by interfacial states. Whatever their values, however, the relevant point here is that a Schottky barrier like that depicted in Fig. 2b) is expected at the bottom interface. At the top interface we would expect a similar situation, even though the work function decreases among the series of electrodes employed ($\Psi_{Pt} \sim 5.65$ eV, $\Psi_{Ni} \sim 5.15$ eV, $\Psi_{Ti} \sim 4.33$ eV, $\Psi_{Cr} \sim 4.5$ eV) [14,27] so that different barrier heights can arise. From this picture, it clearly turns out that, in a perfectly symmetric capacitor (like in the case of Pt/KNN/Pt), there would be two counteracting rectifying barriers giving rise to a symmetric high impedance behavior. The experimental asymmetric J-E curves instead indicate that only one of the two junctions determines the effective rectifying behavior. As the experimental low impedance (high current) state is for $V_{TB} < 0$, from the band diagram of Fig. 2b), it turns out that in this condition the top junction is in reverse mode while the bottom one is in the forward mode. This means that the net rectifying behavior of the MIM device is mainly determined by the bottom junction, between KNN and the Pt(111) template, which is indeed the common contact for all investigated devices, all showing the same polarity of the conduction asymmetry (Fig. 2c). The reason why the top barrier is much less influent, displaying a sort of ohmic behavior, cannot be just related to the different work-function, as the more pronounced

rectifying behavior is found in case of a symmetric Pt/KNN/Pt capacitor. We suggest, instead, that the main explanation relies on the reactivity of metals deposited on KNN to realize the top contacts. This can produce a local heavy doping inducing a thinning of the barrier and almost ohmic transport across it due to tunneling, in analogy with ohmic contacts used in semiconductor technology. Other sources of doping could be the interdiffusion of metals inside the KNN through morphological defects [28], possibly leading also to direct conductive paths. Also, interface oxidation can be called into the cause list. The latter can be verified by using Time of Flight Secondary Ion Mass Spectroscopy (ToF-SIMS) measurements, which can detect various species as a function of the detection depth. For our case it can reveal the sizeable interfacial oxidation for Ti, Ni, Cr, and Pt top layers.

For each M/KNN/Pt stack, we report corresponding metal-oxide complex signals (PtO^-, NiO^-, TiO_2^-, and CrO^- species) in Fig. 3. For KNN, NbO^- ions have been measured. To study the oxygen evolution, O_2^- was followed. The signals (yield) of ions were followed through the stack. We underline, however, that the signals are not calibrated, and thus their relative intensities cannot be used to gain information on chemical concentrations. This is due to the lack of adequate reference samples for conversion. By consequence, the signal intensity of PtO^-, NiO^-, TiO_2^-, and CrO^- species cannot be directly compared to estimate the degree of oxidation for the different metallic species. Nonetheless, the yield for each oxidized species itself is not negligible, thus confirming the presence of oxidation at each interface. For ease of clarity, colored reference bars with depths corresponding to the different material layers have been added on top. In Fig. 3a, starting from the topmost layer, evidence of platinum oxide was found. This is typical of metals developing native oxides as stabilization layers when exposed to the atmosphere. However, just at the interface with KNN, where both
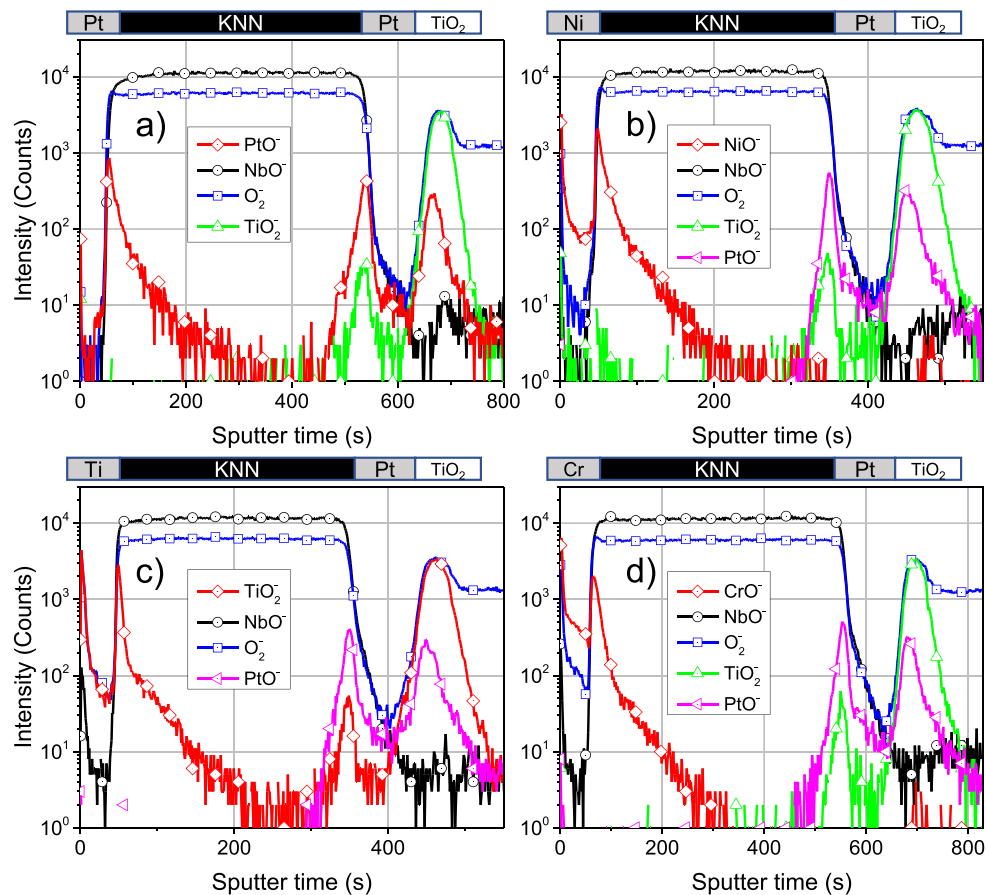

Fig. 3. ToF-SIMS profiles of M-KNN-Pt/TiO$_2$ stacks, where M stands for a) Pt, b) Ni, c) Ti, and d) Cr.

NbO^- and O_2^- species appear, a sudden surge of PtO^- species is observed. It is well known that during the deposition of Pt on oxides, highly reactive nanoparticles can be formed [29]. Considering that the deposition of Pt was done in vacuum (at most in the presence of Ar), the appearance of a platinum oxide is justified only if the oxygen has been scavenged from the KNN layer. Another tantalizing observation is that the profile of NbO^- species just at the interface is a bit lower, while the one of PtO^- decreases rapidly. This could confirm the presence of an oxidized interfacial layer of Pt, scavenging oxygen from KNN. A similar, less intense phenomenon is present at the bottom KNN–Pt interface, where again evidence of oxidized platinum is found. Probably, the oxidation of bottom Pt is also due to oxygen extraction from KNN. Nevertheless, originating from the growth of KNN onto a flat Pt(111) surface, the reduced Pt reactivity can definitely lead to a much lower oxygen vacancy concentration and thus preserve the rectifying behavior of the junction. Remarkably, another surge of platinum oxide is found at the $Pt–TiO_2$ bottom interface. Due to its compatibility with Pt, TiO_2 is used as buffer layer between Pt and SiO_2.

More generally, we deduce that in all the stacks the presence of metal oxides at the corresponding M-KNN interfaces is due to oxygen scavenging from KNN by the metals (Fig. 3 b, c, and d). As in the case of Pt, the presence of metal oxides at the corresponding M-KNN interfaces can only be due to scavenging of oxygen from KNN by the metals. A final interesting observation is the high capability of Ti to diffuse through the Pt bottom layer. Evidence of TiO_2 at the bottom Pt–KNN interface in every stack is seen in Fig. 3c), which probably comes from the $Pt/TiO_2/SiO_2/Si$ substrate. This means that Ti atoms were able to migrate through the bottom Pt layer, and form TiO_2 on it, thus also affecting the chemistry at the bottom interface. Indeed, this phenomenon has been studied by other groups [30]. To summarize, ToF-SIMS analysis supports the creation of oxygen vacancies in KNN through the scavenging of oxygen by different metals to form corresponding oxides at interfaces [10].

To corroborate the picture above, and to check the validity of models assuming uniform charge transport across micro-capacitors, Conductive-AFM (C-AFM) measurements on bare KNN/Pt samples were performed. In Fig. 4a), the image shows the topography of a portion of KNN surface with squared outgrows and agglomerated particles on the surface, which lie at slightly different levels above the surface (10–30 nm). During conductive measurements, bias was applied to the sample (silver-pasted to a metal holder), while the conductive AFM tip was grounded. Note that this corresponds to a bias (V_b) with opposite polarity with respect to the bias (V_{TB}) used for the electric characterization of micro-capacitors. In Fig. 4b, a C-AFM map taken with $V_b = +3$ V shows quite a uniform leakage, corresponding to an average local current of 24.5 nA, with some significant hot spots as large as 71 nA at the edges of just two square outgrows. For smaller crystals and agglomerated particles no current contrast is found. This indicates that large crystals might have a direct connection to the bottom interface and are fully embedded into the KNN matrix below, while the smaller ones do not create a direct conductive path to the bottom Pt electrode. Indeed, this was experimentally confirmed by cross-section SEM images of a KNN/Pt film, like that reported in Fig. 4c. A compact KNN film is seen on top of the Pt bottom layer, but a couple of squared crystals are also found. The smaller one on the left looks as if it is grown out from the KNN surface. Nonetheless, the larger one to the right shows that one edge of the crystal runs all the way down to the bottom KNN–Pt interface. This suggests that some crystal boundaries develop from the very beginning of the film deposition and reach the surface. Interestingly, these boundaries have been associated to high defect concentrations, mainly oxygen vacancies, leading to a high local conductivity like that observed in panel 4 b [25]. Noteworthy, from a statistical analysis of our maps, we found that almost 35% of the total current is flowing through these hot spots. When a negative bias ($V_b = -3$ V) was applied to the sample, the C-AFM image did not show any significant contrast at such hot spots, though. Moreover, although the work function of the diamond
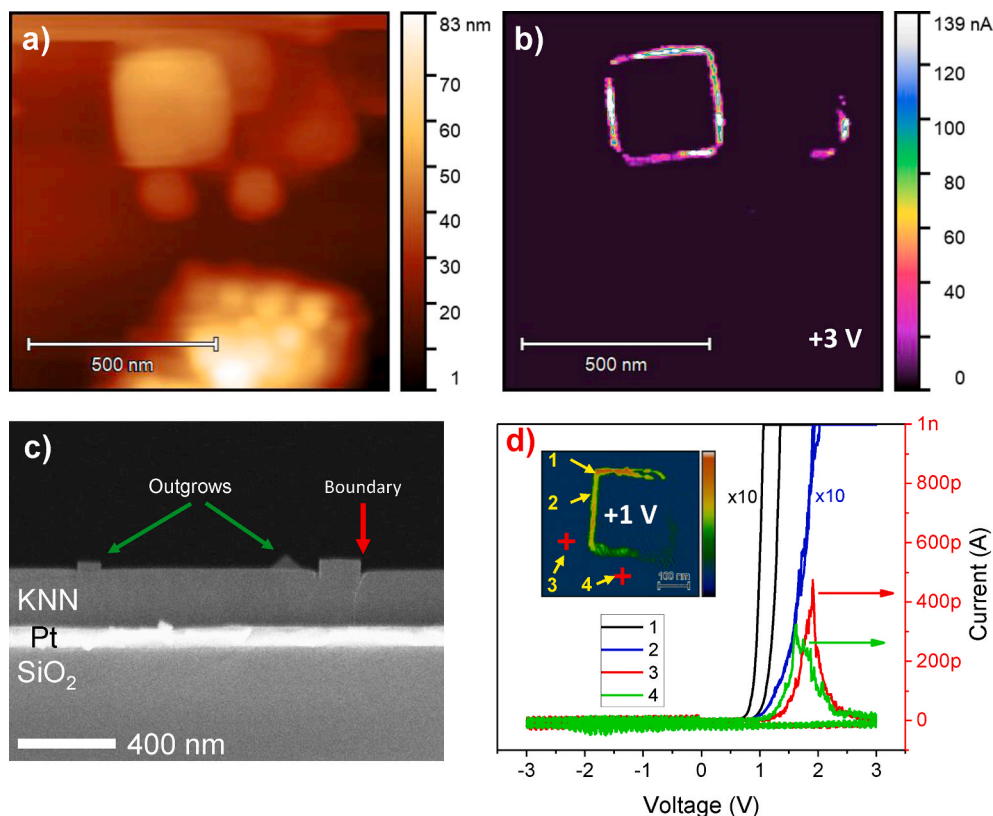

Fig. 4. a) AFM topography of bare KNN surface on bottom Pt electrode, b) conductive-AFM image of the same area with variation in leakage around crystal borders, c) SEM cross-section image of a KNN/Pt/SiO$_2$ film and, d) I–V characteristics of four spots on the film as measured by C-AFM.

tip is high (about 5.5 eV), the emission could be tip-limited mostly when the sample is positively biased, but not so much when it is negatively biased [31]. Therefore, also with C-AFM we find a rectifying behavior coherent with J-E curves on micro-capacitors: a sizable current is measured for $V_b > 0$, corresponding to $V_{TB} < 0$, in full agreement with Fig. 1. As here the top contact is provided by the AFM tip while the bottom KNN/Pt(111) interface is the same as that of micro-capacitors, C-AFM results confirm that the rectifying behavior of micro-capacitors is determined by the bottom interface.

To gain a deeper insight into the local conduction mechanisms, we measured the current-voltage characteristics of the hot spots at the edges of crystals and of the more homogeneous KNN film, at the four points indicated by the numbers in the inset of Fig. 4d. When the tip is placed on the conductive edge of one crystal (points 1 and 2), and the voltage is swept in between −3 V and +3 V, a large current saturating the AFM pre-amplifier is seen only for positive sample bias, while for negative bias the current is within the noise, thus clearly displaying the rectifying behavior previously seen in the current maps. Interestingly, for a couple of measurements on less leaky spots (points 3 and 4), an asymmetric I-V_b curve is also measured, displaying a peak for $V_b > 0$ and much smaller current for negative bias. Even though many complex phenomena can contribute to this peak, like charge migration and high conductivity at ferroelectric domain walls [32], its position at 56 kV/cm is very close to the coercive field for KNN we measured on similar films [8] so that it could be related to the local ferroelectric switching of KNN. The fact that a similar peak does not appear for negative bias can be explained on the basis of the rectifying behavior of the bottom interface. For $V_b < 0$, the junction is in reverse mode, which means that a sizable portion of the applied voltage drops across the junction itself, mainly located in the space charge region responsible for the small signal capacitance reported above. By consequence, the effective voltage applied across the KNN film is reduced, and ferroelectric switching is hampered. This result is relevant as it sheds light on the impact of asymmetric leakage on the ferroelectric switching of piezoelectric materials. Overall, C-AFM measurements indicate that the asymmetry of the current measured in micro-capacitors is not peculiar to hot spots; it is a common phenomenon seen also on less leaky points which is compatible with the presence of a Schottky-like barrier at the bottom interface.

4. Discussion

From the analysis of our experimental results, the simplified concentrated parameters model of Fig. 2c emerges, with a diode representing the rectifying bottom interface, a complex impedance describing the bulk KNN behavior, and a resistor which represents the "ohmic behavior" of the top contact. With reference to this model, we can qualitatively explain the J-E curves of Fig. 1. For small bias (region C) an almost ohmic behavior is found in case of Ti and Cr electrodes. As a matter of fact, the equivalent resistivities for positive and negative bias ($\rho+$ and $\rho-$) estimated from a linear fit of the J-E curves from 0 to ± 5 kV/cm from the minimum, are essentially the same (see Table 1). This is not always true for Pt and Ni. Even though the resistivity is higher, in half of the investigated Pt and Ni devices we found a more ohmic, but still asymmetric, behavior like that of Cr and Ti. In the other half (like those giving the J-E curves in Fig. 1) the more pronounced rectifying behavior reflects in a sizable small-bias asymmetry so that a linear fit for positive bias is not meaningful, as expected for a true diode in series with

a resistance.

The fact that for Cr and Ti the equivalent resistivities are much smaller than for Pt and Ni is in agreement with the higher concentration of oxygen vacancies due to oxygen scavenging for the latter electrodes, or to the tendency of Ti and Cr to diffuse into the KNN films, as reported below.

Moving towards larger positive bias ($V_{TB} > 0$), we enter region D where the leakage current is limited by the bottom interface in reverse bias and a plateau appears for Pt and Ni. This is the region where small signal capacitance measurements were carried out, confirming the presence of a space-charge region. By further increasing V_{TB}, we assist to a remarkable increase of the leakage current which could be associated to a sort of breakdown of the bottom junction, due to the activation of additional conduction processes (region E). For Ti and Cr, we do not see a distinction between regions D and E, most probably because of the higher reactivity of Ti and Cr giving rise to high leakage also at small positive bias. We should also mention that also for some Pt and Ni pads we did not find a plateau but just a curve like those measured for Ti and Cr, but with less current density. This variability can be ascribed to the random distribution of hot spots for conduction associated to defects like those in Fig. 4b under different pads. The different behavior found for Pt–Ni and Ti–Cr can be explained considering that, apart from creation of oxygen vacancies at the top interface, other effects can arise. Titanium can diffuse through grain boundaries of KNN to the full thickness of KNN [28] and produce oxygen vacancies deep within the insulator. It is thus very likely that different surface states appear at the bottom KNN–Pt interface depending on the choice of the top electrode material [16], altering the barrier height by Fermi level pinning and affecting the rectifying behavior. The enthalpies of formation of oxides of Pt, Ni, Ti, and Cr are −80, −240, −945, and −1128 kJ/mol at standard conditions. Therefore, it is expected that Cr and Ti can more easily scavenge oxygen from KNN at the top interface to form the corresponding oxides. For Ni and Pt, the oxidation process is energetically less favorable, but the higher reactivity of nanoparticles formed at the early stage of the growth of metals on oxides is expected to produce oxygen vacancies in the topmost KNN layers, in analogy with what has been observed for other noble metal/perovskite interfaces [29], with concentration high enough to generate a local heavy doping. On the other hand, the sizable difference in the enthalpies of formation is expected to reflect also in a marked difference in the bulk doping of the KNN film by oxygen vacancies, which is connected to the intrinsic leakage. This is clear looking at the absolute values of the leakage currents reported in Fig. 1, which are definitely lower for Pt and Ni than for Ti and Cr, both for positive and negative bias.

Coming back to our concentrated parameters model, for $V_{TB} < 0$ the bottom junction is in the forward mode, so that the applied voltage effectively drops across the KNN film and we assist to a steep current growth reflecting the intrinsic leakage mechanisms within the bulk of the film (region B of Fig. 1). For larger negative values of V_{TB}, we see a reduction of slope indicating that another phenomenon is limiting the leakage current. In the theory of metal-insulator interfaces, Schottky and Poole-Frenkel emission models are frequently used to interpret bias regime at high applied voltages [33,34]. The first is an electrode-limited conduction mechanism in which the most important limiting factor is the work-function of the metal used, determining the effective barrier to be overcome to inject electrons from the metal into the insulator. The second is a bulk-limited conduction mechanism describing how electrons (or mobile, negatively charged defects) are emitted from traps in the dielectric thanks to a field-induced reduction of their potential barrier. Both have more relevance at high applied electric fields and increasing temperatures, where excitation of charges is more efficient. In our case, as we are dealing with films with thickness (300 nm) larger than the electron mean free path, both effects are expected to play a role. Interestingly enough, in this regime both the Schottky model corrected with the introduction of the effect of bulk traps and the pure Poole-Frenkel model predicts a linear behavior in the plot of Ln (J/E) vs

Table 1
Estimated resistivities for positive ($\rho+$) and negative ($\rho-$) applied bias near the minimum of the leakage current. In case of Pt and Ni the pronounced rectifying behavior for VTB >0 impedes a realistic estimate.

	Pt	Ni	Ti	Cr
$\rho+$ ($\Omega\cdot$cm)	/	/	$8\cdot10^5$	$8\cdot10^4$
$\rho-$ ($\Omega\cdot$cm)	$8.8\cdot10^8$	$5.6\cdot10^8$	$7\cdot10^5$	$8\cdot10^4$

(E)$^{1/2}$ [21,34]. As a matter of fact, for most of measurements on different pads, we found a linear behavior as predicted by the model, especially for Pt, and Ni, thus confirming that at higher negative voltages Schottky emission at the top electrode and Poole-Frenkel emission could be the main phenomena limiting the leakage current at high negative bias (see Fig. 5). However, the extraction of physical quantities like the dielectric constant and the effective barrier height from this kind of analysis is prevented due to the huge variability of experimental results which can be understood if one considers that a sizable fraction of current is localized at the edges of crystalline grains (see Fig. 4b), with random distribution under different metallic contacts.

Our results shed light on the impact of the choice of different electrodes on the overall performance of piezoelectric devices, confirming that Pt and Ni are somewhat equivalent, while highly reactive materials like Ti and Cr must be avoided. Furthermore, the fact that the top interface behaves like an "ohmic contact", most probably due to the creation of oxygen vacancies, suggests that the usage of direct metallic contacts should be avoided in any case, to minimize the creation of oxygen vacancies by scavenging by metals. The creation of a Schottky-like barrier at the bottom interface, also in case of more inert materials like Pt and Ni, revealed to be highly critical for the switching of the ferroelectric polarization and operation of the piezoelectric materials. In fact, our local I(V) curves measured by C-AFM show that a peak current associated to the ferroelectric switching is seen only for a bias putting the rectifying junction in the forward mode. For the opposite bias, a large fraction of the applied voltage drops across the Schottky-like junction, thus hampering the switching as the effective electric field across the KNN film is reduced. Clearly, this effect is more relevant for leaky piezoelectric materials, as for ideal dielectric with low leakage there will be no voltage drop across the Schottky barrier.

From a practical perspective, as ferroelectric and piezoelectric material, KNN should be highly insulating and give rise to ohmic contacts with bottom and top electrodes, without interfacial depletion regions. In such case, the electrode-KNN interface easily provides balancing charges to screen polarization charges from KNN. The conduction is bulk-limited by KNN and, if properly insulating, low leakage is ensured [9,35]. For sizable doping, as discussed in the present paper, more complex phenomena appear due to the creation of depletion regions at the interfaces with electrodes. In case of very large doping under the top electrode an ohmic behavior can be achieved [36], similarly to what is done in semiconductor technology, but this must be avoided if the high doping is obtained by uncontrolled phenomena like oxygen scavenging by metallic electrodes. In fact, our results suggest that oxygen vacancies

also affect the bulk of the insulator, which transforms in a doped semiconductor. In this scenario, apart from a sizable increase of leakage, the effective electric field across the piezoelectric material is no more uniform, due to the creation of a wide depletion region at the bottom interface which causes an asymmetric conduction behavior and ferroelectric switching. Overall, our results point to the need of minimizing Schottky-like barriers by interface engineering which prevents oxygen scavenging by metallic electrodes, e.g. by inserting a conducting oxide, in order to avoid the asymmetric operation of the piezo material.

5. Conclusions

In this paper we described the mechanisms leading to asymmetric leakage currents in M/KNN/Pt(111) micro-capacitors, where M stands for Pt, Ni, Ti, and Cr. For all metals used as top electrode, we found a rectifying behavior with leakage currents for negative top-bottom voltage (V_{TB}) much higher than for negative bias, both from macroscopic measurements on micro-capacitors and from local conductive AFM measurements. We ascribed this behavior to the presence of a rectifying Schottky-like junction at the bottom interface between the KNN film and the Pt(111) substrate, as confirmed by small signal capacitance measurements which are consistent with space charge accumulation at the same interface. Noteworthy, the rectifying behavior is more pronounced in symmetric Pt/KNN/Pt capacitors, thus pointing out that the origin of the asymmetry cannot be purely ascribed to the different work functions of top and bottom electrodes. As the leakage current increases with the chemical reactivity of the electrodes, following the enthalpies of formation of related oxides, we suggest that the main driving mechanism here is connected to oxygen scavenging during the deposition of KNN, with the subsequent creation of oxygen vacancies which act as donors. As a matter of fact, significant oxidation of top electrode metals was found at the top metal-KNN interfaces by ToF-SIMS. This gives rise to the creation of "ohmic contacts" at the heavily-doped top interface and to a non-uniform doping within the KNN film, leading both to an increase of leakage and to the creation of a depletion region at the bottom interface, acting as a rectifying Schottky barrier. The potential impact of this asymmetric leakage on the ferroelectric switching and bipolar piezo operation is discussed, pointing to the need of minimizing asymmetric potential barriers at the top and bottom interfaces to reach a symmetric operation of the piezo-material.

CRediT authorship contribution statement

C. Groppi: Writing – original draft, Methodology, Investigation, Formal analysis, Data curation, Conceptualization. **F. Maspero:** Writing – original draft, Supervision, Formal analysis, Data curation. **A. Rovelli:** Methodology, Investigation. **M. Asa:** Writing – original draft, Supervision, Methodology, Conceptualization. **G. Malavena:** Formal analysis, Data curation. **C. Monzio Compagnoni:** Methodology, Formal analysis, Data curation. **E. Albisetti:** Resources, Investigation, Data curation. **S. Vangelista:** Data curation, Formal analysis, Resources, Writing – original draft, Writing – review & editing. **M.A. Badillo-Ávila:** Writing – original draft, Validation, Methodology, Formal analysis, Data curation. **R. Bertacco:** Writing – original draft, Validation, Supervision, Resources, Project administration, Funding acquisition, Formal analysis, Conceptualization.

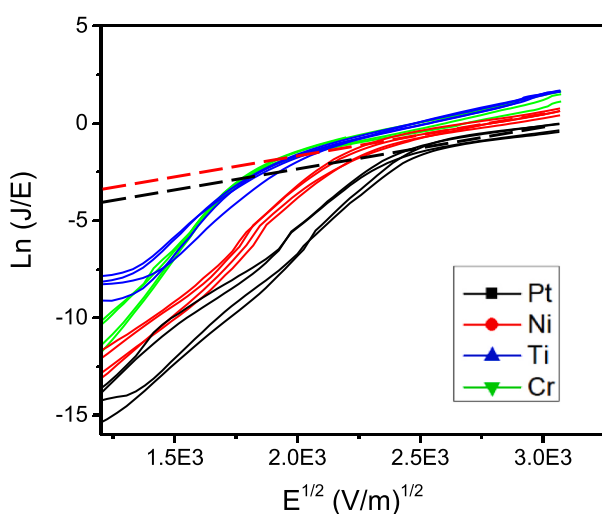## Declaration of competing interest

Fig. 5. Ln (J/E) vs. |E|$^{1/2}$ for fitting at high E of Schottky-Simmons emission due to electrode work function and traps in KNN for forward bias ($V_{TB} < 0$).

References

[1] K. Xu, J. Li, X. Lv, J. Wu, X. Zhang, D. Xiao, J. Zhu, Superior piezoelectric properties in potassium-sodium niobate lead-free ceramics, Adv. Mater. 28 (2016) 8519–8523, https://doi.org/10.1002/adma.201601859.

[2] J. Rödel, K.G. Webber, R. Dittmer, W. Jo, M. Kimura, D. Damjanovic, Transferring lead-free piezoelectric ceramics into application, J. Eur. Ceram. Soc. 35 (2015) 1659–1681, https://doi.org/10.1016/j.jeurceramsoc.2014.12.013.

[3] H.C. Thong, C. Zhao, Z.X. Zhu, X. Chen, J.F. Li, K. Wang, The impact of chemical heterogeneity in lead-free (K,Na)NbO3 piezoelectric perovskite: ferroelectric phase coexistence, Acta Mater. 166 (2019) 551–559, https://doi.org/10.1016/j.actamat.2019.01.012.

[4] Y. Quan, W. Ren, G. Niu, L. Wang, J. Zhao, N. Zhang, M. Liu, Z.-G. Ye, L. Liu, T. Karaki, Large piezoelectric strain with superior thermal stability and excellent fatigue resistance of lead-free potassium sodium niobate-based grain orientation-controlled ceramics, ACS Appl. Mater. Interfaces 10 (2018) 10220–10226, https://doi.org/10.1021/acsami.8b01554.

[5] W. Chen, Z. Yu, J. Pang, P. Yu, G. Tan, C. Ning, Fabrication of biocompatible potassium sodium niobate piezoelectric ceramic as an electroactive implant, Materials 10 (2017) 345, https://doi.org/10.3390/ma10040345.

[6] R. Chen, K.K. Shung, T. Ma, Q. Zhou, L. Jiang, T. Zhang, T. Matsuoka, M. Yamazaki, X. Qian, G. Lu, A. Safari, J. Zhu, Eco-friendly highly sensitive transducers based on a new KNN–NTK–FM lead-free piezoelectric ceramic for high-frequency biomedical ultrasonic imaging applications, IEEE Trans. Biomed. Eng. 66 (2019) 1580–1587, https://doi.org/10.1109/TBME.2018.2876063.

[7] D. Khare, A. Singh, A.K. Dubey, Influence of Na and K contents on the antibacterial response of piezoelectric biocompatible NaxK1-xNbO3 (x = 0.2–0.8), Mater, Today Commun 27 (2021), 102317, https://doi.org/10.1016/j.mtcomm.2021.102317.

[8] C. Groppi, L. Mondonico, F. Maspero, C. Rinaldi, M. Asa, R. Bertacco, Effect of substrate preparation on the growth of lead-free piezoelectric (K0.5Na0.5)NbO3 on Pt(111), J. Appl. Phys. 129 (2021), 194102, https://doi.org/10.1063/5.0050038.

[9] S. Sharma, A. Kumar, V. Gupta, M. Tomar, Influence of top metal electrode on electrical properties of pulsed laser deposited lead-free ferroelectric K0.35Na0.65NbO3 thin films, Mater. Sci. Semicond. Process. 103 (2019), 104618, https://doi.org/10.1016/j.mssp.2019.104618.

[10] L. Michalas, A. Khiat, S. Stathopoulos, T. Prodromakis, Electrical characteristics of interfacial barriers at metal—TiO2 contacts, J. Phys. D Appl. Phys. 51 (2018), 425101, https://doi.org/10.1088/1361-6463/aadbd2.

[11] N. Alaei-Sheini, M. Rohani, Resistive switching in platinum/titanium dioxide Schottky diode, in: 2019 27th Iran. Conf. Electr. Eng., IEEE, 2019, pp. 442–445, https://doi.org/10.1109/IranianCEE.2019.8786517.

[12] L. Su, Z. Guan, Q. Liu, Y. Zhu, Ohmic-Schottky conversion of ZnO/metal contact modulated by a plasma surface treatment method, Results Mater 15 (2022), 100290, https://doi.org/10.1016/j.rinma.2022.100290.

[13] H.N. Al-Shareef, A.I. Kingon, X. Chen, K.R. Bellur, O. Auciello, Contribution of electrodes and microstructures to the electrical properties of Pb(Zr0.53Ti0.47)O3 thin film capacitors, J. Mater. Res. 9 (1994) 2968–2975, https://doi.org/10.1557/JMR.1994.2968.

[14] L. Pintilie, I. Vrejoiu, D. Hesse, M. Alexe, The influence of the top-contact metal on the ferroelectric properties of epitaxial ferroelectric Pb(Zr0.2Ti0.8)O3 thin films, J. Appl. Phys. 104 (2008), 114101, https://doi.org/10.1063/1.3021293.

[15] I. Pintilie, C.M. Teodorescu, C. Ghica, C. Chirila, A.G. Boni, L. Hrib, I. Pasuk, R. Negrea, N. Apostol, L. Pintilie, Polarization-control of the potential barrier at the electrode interfaces in epitaxial ferroelectric thin films, ACS Appl. Mater. Interfaces 6 (2014) 2929–2939, https://doi.org/10.1021/am405508k.

[16] T. Li, G. Wang, K. Li, N. Sama, D. Remiens, X. Dong, Influence of LNO top electrodes on electrical properties of KNN/LNO thin films prepared by RF magnetron sputtering, J. Am. Ceram. Soc. 96 (2013) 787–790, https://doi.org/10.1111/jace.12047.

[17] A. Madani, R. Ben Mrad, A.N. Sinclair, Characterization of RF sputtered thin film potassium sodium niobate (KNN) with silicon and nickel electrodes, Microsyst. Technol. 23 (2017) 1943, https://doi.org/10.1007/s00542-016-3106-x. –1948.

[18] Y. Sun, F. Guo, J. Chen, S. Zhao, Improved ferroelectric and photovoltaic properties of BiMnO3 modified lead-free K0.5Na0.5NbO3 solid-solution films, Appl. Phys. Lett. 111 (2017) 1–6, https://doi.org/10.1063/1.5006643.

[19] G.H. Khorrami, A. Kompany, A. Khorsand Zak, Structural and optical properties of (K,Na)NbO3 nanoparticles synthesized by a modified sol–gel method using starch media, Adv. Powder Technol. 26 (2015) 113–118, https://doi.org/10.1016/j.apt.2014.08.013.

[20] S.A. Mojarad, J.P. Goss, K.S.K. Kwa, Z. Zhou, R.A.S. Al-Hamadany, D.J.R. Appleby, N.K. Ponon, A. O'Neill, Leakage current asymmetry and resistive switching behavior of SrTiO3, Appl. Phys. Lett. 101 (2012) 173507, https://doi.org/10.1063/1.4764544.

[21] S.A. Mojarad, K.S.K. Kwa, J.P. Goss, Z. Zhou, N.K. Ponon, D.J.R. Appleby, R.A.S. Al-Hamadany, A. O'Neill, A comprehensive study on the leakage current mechanisms of Pt/SrTiO3/Pt capacitor, J. Appl. Phys. 111 (2012), 014503, https://doi.org/10.1063/1.3673574.

[22] F. El Kamel, P. Gonon, C. Vallée, Experimental evidence for the role of electrodes and oxygen vacancies in voltage nonlinearities observed in high-k metal-insulator-metal capacitors, Appl. Phys. Lett. 91 (2007), 172909, https://doi.org/10.1063/1.2803221.

[23] Y. Huan, X. Wang, T. Wei, J. Xie, Z. Ye, P. Zhao, L. Li, Defect engineering of high-performance potassium sodium niobate piezoelectric ceramics sintered in reducing atmosphere, J. Am. Ceram. Soc. 100 (2017) 2024–2033, https://doi.org/10.1111/jace.14721.

[24] F. Hussain, I. Sterianou, A. Khesro, D.C. Sinclair, I.M. Reaney, p-Type/n-type behaviour and functional properties of KxNa(1-x)NbO3 (0.49 ≤ x ≤ 0.51) sintered in air and N2, J. Eur. Ceram. Soc. 38 (2018) 3118–3126, https://doi.org/10.1016/j.jeurceramsoc.2018.03.013.

[25] X. Wang, Y. Huan, Z. Wang, X. Lin, S. Huang, T. Wei, L. Li, X. Wang, Electrical conduction and dielectric relaxation mechanisms in the KNN-based ceramics, J. Appl. Phys. 126 (2019), 104101, https://doi.org/10.1063/1.5110582.

[26] W.-C. Yang, B.J. Rodriguez, A. Gruverman, R.J. Nemanich, Polarization-dependent electron affinity of LiNbO3 surfaces, Appl. Phys. Lett. 85 (2004) 2316–2318, https://doi.org/10.1063/1.1790604.

[27] B. Ofuonye, J. Lee, M. Yan, C. Sun, J.M. Zuo, I. Adesida, Electrical and microstructural properties of thermally annealed Ni/Au and Ni/Pt/Au Schottky contacts on AlGaN/GaN heterostructures, Semicond. Sci. Technol. 29 (2014), https://doi.org/10.1088/0268-1242/29/9/095005.

[28] P.C. Goh, K. Yao, Z. Chen, Titanium diffusion into (K0.5Na0.5)NbO 3 thin films deposited on Pt/Ti/SiO2/Si substrates and corresponding effects, J. Am. Ceram. Soc. 92 (2009) 1322–1327, https://doi.org/10.1111/j.1551-2916.2009.03058.x.

[29] S. Brivio, C. Magen, A.A. Sidorenko, D. Petti, M. Cantoni, M. Finazzi, F. Ciccacci, R. De Renzi, M. Varela, S. Picozzi, R. Bertacco, Effects of Au nanoparticles on the magnetic and transport properties of La0.67Sr0.33MnO3 ultrathin layers, Phys. Rev. B 81 (2010), 094410, https://doi.org/10.1103/PhysRevB.81.094410.

[30] A. Ababneh, A.N. Al-Omari, A.M.K. Dagamseh, M. Tantawi, C. Pauly, F. Mücklich, D. Feili, H. Seidel, Electrical and morphological characterization of platinum thin-films with various adhesion layers for high temperature applications, Microsyst. Technol. 23 (2017) 703–709, https://doi.org/10.1007/s00542-015-2715-0.

[31] C. Villeneuve-Faure, K. Makasheva, L. Boudou, G. Teyssedre, Charge injection in thin dielectric layers by atomic force microscopy: influence of geometry and material work function of the AFM tip on the injection process, Nanotechnology 27 (2016), 245702, https://doi.org/10.1088/0957-4484/27/24/245702.

[32] W. Yang, G. Tian, H. Fan, Y. Zhao, H. Chen, L. Zhang, Y. Wang, Z. Fan, Z. Hou, D. Chen, J. Gao, M. Zeng, X. Lu, M. Qin, X. Gao, J. Liu, Nonvolatile ferroelectric-domain-wall memory embedded in a complex topological domain structure, Adv. Mater. 34 (2022), 2107711, https://doi.org/10.1002/adma.202107711.

[33] A. Türüt, Oncurrent-voltage and capacitance-voltage characteristics of metal-semiconductor contacts, TURKISH J. Phys. 44 (2020) 302–347, https://doi.org/10.3906/fiz-2007-11.

[34] F.C. Chiu, A review on conduction mechanisms in dielectric films, Adv. Mater. Sci. Eng. 2014 (2014), https://doi.org/10.1155/2014/578168.

[35] T. Li, S. Dai, L. Xu, Y. Liu, H. Zhuo, K. Wang, H. Wang, F. Chen, Electrical property and phase transition analysis of KNN-based lead-free ferroelectric films, Mater. Res. Express 9 (2022), 056403, https://doi.org/10.1088/2053-1591/ac6b8c.

[36] J.J. Yang, M.D. Pickett, X. Li, D.A.A. Ohlberg, D.R. Stewart, R.S. Williams, Memristive switching mechanism for metal/oxide/metal nanodevices, Nat. Nanotechnol. 3 (2008) 429–433, https://doi.org/10.1038/nnano.2008.160.